Biochimica et Biophysica Acta 1778 (2008) 2058–2068

Contents lists available at ScienceDirect

Biochimica et Biophysica Acta

journal homepage: www.elsevier.com/locate/bbamem

Nanoscale membrane activity of surfactins: Influence of geometry, charge and hydrophobicity

Grégory Francius [a], Samuel Dufour [b], Magali Deleu [b], Michel Paquot [b], Marie-Paule Mingeot-Leclercq [c], Yves F. Dufrêne [a,*]

[a] Unité de chimie des interfaces, Université catholique de Louvain, Croix du Sud 2/18, B-1348 Louvain-la-Neuve, Belgique
[b] Unité de chimie industrielle, Faculté universitaire des sciences agronomiques de Gembloux, 2, passage des déportés, B-5030 Gembloux, Belgique
[c] Unité de Pharmacologie Cellulaire et Moléculaire, Université catholique de Louvain, UCL 73.70, Avenue E. Mounier 73, B-1200, Brussels, Belgique

ARTICLE INFO

Article history:
Received 18 January 2008
Received in revised form 21 March 2008
Accepted 31 March 2008
Available online 11 April 2008

Keywords:
AFM
Analogs
Micelles
Supported lipid membranes
Surfactin

ABSTRACT

We used real-time atomic force microscopy (AFM) to visualize the interactions between supported lipid membranes and well-defined surfactin analogs, with the aim to understand the influence of geometry, charge and hydrophobicity. AFM images of mixed dioleoylphosphatidylcholine/dipalmitoylphosphatidylcholine (DOPC/DPPC) bilayers recorded after injection of cyclic surfactin at 1 mM, i.e. well-above the critical micelle concentration, revealed a complete solubilization of the bilayers within 30 min. A linear analog having the same charge and acyl chains was able to solubilize DOPC, but not DPPC, and to promote redeposition leading eventually to a new bilayer. Increasing the charge of the polar head or the length of the acyl chains of the analogs lead to the complete solubilization of both DOPC and DPPC, thus to a stronger membrane activity. Lastly, we found that at low surfactin concentrations (40 μM), DPPC domains were always resistant to solubilization. These data demonstrate the crucial role played by geometry, charge and hydrophobicity in modulating the membrane activity (solubilization, redeposition) of surfactin. Also, this study suggests that synthetic analogs are excellent candidates for developing new surfactants with tunable, well-defined properties for medical and biotechnological applications.

1. Introduction

The increasing resistance of microbes to conventional antibiotics is a major concern that has led to an intense search for new types of drugs. Among these, the lipopeptide surfactin produced by *Bacillus subtilis* [1] is particularly promising in view of its strong biological activities [2–8]. Surfactin consists of a heptapeptide headgroup with the sequence Glu-Leu-D-Leu-Val-Asp-D-Leu-Leu closed to a lactone ring by a C13–15 β-hydroxy fatty acid (Fig. 1). The peptide ring adopts a "horse-saddle" structure in solution with the two charged residues forming a "claw," which is a potential binding site for divalent cations [9]. On the opposite side of the ring, the fatty acyl chain may extend into a micellar structure or into a lipid bilayer [10].

Surfactins are thought to kill target cells by permeabilizing their membranes via a so-called detergent-like action [10–13]. In general, detergents induce a positive spontaneous curvature in membranes, leading to a disordering of the acyl chains a reduction in membrane thickness and lateral packing density, and a loss of mechanical membrane stability. To explore the structure–function relationships of surfactin, Dufour et al. [8] synthesized linear surfactin analogs based on the pattern of a natural cyclic surfactin with a C14 acyl chain (SNC14). They found that, compared to the cyclic natural surfactin, analogs have lower surface and hemolytic activities. These synthetic analogs appear as an interesting research tool to investigate the influence of subtle structural variations on the membrane activity of surfactin.

During the past decade, atomic force microscopy (AFM) has proved to be a powerful technique to image supported lipid membranes [14,15] and their interaction with peptides [16,17], proteins [18], drugs [19], solvents [20], and detergents [21]. Here, we used the technique to investigate the ability of various well-defined surfactin molecules to alter the nanoscale organization of supported bilayers. We compared the behavior of the natural cyclic surfactin SNC14 with that of synthetic linear analogs differing in their charge (2 vs 3 acid groups) and acyl chains (10, vs 14 and 18 carbons), and tested the effect of surfactin concentration (1000, 40 and 3 μM). The data emphasize the crucial role played by the peptide cycle, charge, and acyl chain length in modulating the membrane activity (solubilization, redeposition) of surfactin.

2. Materials and methods

2.1. Materials

Dioleoylphosphatidylcholine (DOPC) and dipalmitoylphosphatidylcholine (DPPC), were purchased from Sigma (St. Louis, MO). The different surfactin analogs were

* Corresponding author. Tel.: +32 10 47 36 00; fax: +32 10 47 20 05.
E-mail address: Yves.Dufrene@uclouvain.be (Y.F. Dufrêne).

0005-2736/$ – see front matter © 2008 Elsevier B.V. All rights reserved.
doi:10.1016/j.bbamem.2008.03.023

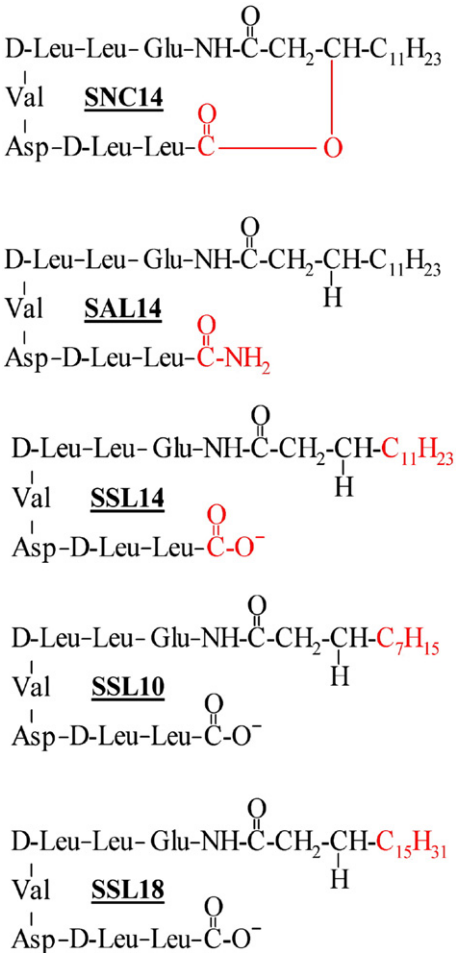

Fig. 1. Structure of the five surfactins investigated here (see text for details).

produced as previously described [8]. Briefly, SAL14, SSL10, SSL14 and SSL18 were produced by Fmoc SPPS. The fatty acid chain was added by the reaction of fatty anhydride on the peptidic moiety. All these products were purified by preparative HPLC up to 95% (purity estimated by HPLC-UV). Identification and purity of the product were evaluated using infrared spectroscopy, amino-acid analysis, rp-HPLC and MALDI-TOF MS spectrometry. Their characteristics (structure, molar mass, CMC and solubility) are shown in Table 1. Surfactins were diluted at 1000, 40 and 3 μM concentrations in buffer solution of Tris/NaCl (10 mM Tris, 150 mM NaCl, pH 7.4). Two different solutions were used for preparing and imaging the lipid bilayers, i.e. Tris/NaCl/$CaCl_2$ (10 mM Tris, 150 mM NaCl, 3 mM $CaCl_2$, pH 7.4), and Tris/NaCl (10 mM Tris, 150 mM NaCl, pH 7.4).

2.2. Preparation of supported lipid bilayers

Supported bilayers were prepared as follows. Lipid mixtures were dissolved in $CHCl_3$ in glass tubes, evaporated with nitrogen and dried in a desiccator under vacuum for 2 h. The lipids were then resuspended from the walls of the glass tube by vigorous vortexing in Tris/NaCl/$CaCl_2$ buffer (~5 mL). To obtain small unilamellar vesicles (SUVs), the suspension was sonicated to clarity (3 cycles of 2 min) using a 500 W probe sonicator (Fisher Bioblock Scientific, France; 35% of the maximal power; 13 mm probe diameter) while keeping the suspension in an ice bath and the suspension was finally filtered on 0.2 μm nylon filters (Whatman Inc., USA) to eliminate titanium particles. The SUV solution was then put into contact with freshly-cleaved mica substrates for 45 min at 60 °C. After slowly cooling down the system to room temperature, the samples were carefully rinsed to remove the SUV excess using a Tris/NaCl solution. Then, samples were transferred into the AFM liquid cell while avoiding dewetting. Mica slides were fixed to a steel sample puck (Digital Instruments, Santa Barbara, CA) using Epo-Tek 377 glue (Gentec Benelux, B-1410 Waterloo, Belgium) before being cleaved.

2.3. AFM imaging

AFM measurements were made at room temperature (~23 °C) in Tris/NaCl buffer solution (10 mM Tris, 150 mM NaCl, pH 7.4), using a commercial microscope (Nanoscope III Multimode AFM, Veeco Metrology Inc, Santa Barbara, CA). Contact mode topographic images were taken in the constant-deflection mode using oxide-sharpened microfabricated Si_3N_4 cantilevers (Veeco Metrology Group) with typical radius of curvature of 20 nm and spring constant of 0.01 N/m (manufacturer specified). The applied force was kept at values <200 pN and the scan rate was 4-6 Hz and AFM images were flattened (flattening order of 3). For each condition, experiments were done at least in duplicate.

3. Results and discussion

We have used real-time AFM imaging to explore the interaction of supported DOPC/DPPC bilayers with various surfactin molecules differing in the geometry and charge of their polar head and in the length of their acyl chain. Fig. 1 and Table 1 present the main characteristics of the five surfactins investigated here. The natural surfactin SNC14 is the only molecule possessing a cyclic structure. It shows a critical micellar concentration (CMC) of 62 μM which is surprisingly high compared to the 7–9 μM values reported for surfactin mixtures [10,22]. This difference is essentially due to differences in purity, i.e. here we worked with purified SNC14 while the above studies used surfactin mixtures containing surfactins of different lengths. The linear analog SAL14 has the same chain length and charged groups in neutral buffer as SNC14. Yet, it shows much higher CMC (~400 μM), indicating that the loss of the cyclic structure does not suppress but lowers the surface-active properties of the molecules and confirming the notion that the cyclic horse saddlelike structure of surfactin plays an important role in conferring its surface-active properties by favoring the existence of distinct polar and apolar domains. SSL10, SSL14 and SSL18 have an additional charged group and differ by the length of their acyl chain (10, 14 and 18 carbon atoms, respectively). The CMC decreases dramatically as the acyl chain length increases reflecting stronger cohesive hydrophobic forces.

Topographic images of mixed DOPC/DPPC (1:1, mol/mol) bilayer supported on mica recorded in buffer solution (Fig. 2) showed the coexistence of two phases, the lighter and darker levels corresponding to DPPC- and DOPC-enriched phases respectively [14,19]. The step height measured between the two phases was 1.2±0.1 nm (see vertical cross-section) and resulted from a difference in the thickness and mechanical properties of the DOPC and DPPC films [23].

3.1. Cyclic surfactin SNC14 induces the complete solubilization of DOPC/DPPC bilayers

Topographic images of the same bilayer region were recorded after incubation for 5, 10, 20, 30, 60, 120, 180 and 240 min with SNC14 at 1 mM, i.e. well-above the CMC (Fig. 2). After only 5 min, the entire surface was covered with small particles, 5.7±0.25 nm in height (see vertical cross-section) and some small DPPC islands remained visible. Whether the observed particles reflect mixed lipid/surfactin micelles, or DPPC aggregates physically spread over the surface by the action of the scanning AFM tip remain to be elucidated. After 30 min, the lipid particles and islands completely disappeared, revealing the smooth underlying mica surface. This behaviour is reminiscent of that reported for the detergent Triton X-100 at the same concentration [24], except that for Triton no particles were seen and DPPC domains were solubilized more slowly. Taken together, these observations indicate

Table 1
Characteristics of the five surfactins investigated here

Surfactin	SNC14	SAL14	SSL14	SSL10	SSL18
Structure	Cyclic	Linear	Linear	Linear	Linear
Charge	2	2	3	3	3
Acyl chain (# C atoms)	14	14	14	10	18
Molar mass (g/mol)	1022	1023	967	1079	1039
CMC (μM)	62	401	302	1114	8

that SNC14 causes the rapid solubilization of both DOPC and DPPC, presumably by a detergent-like effect involving insertion of SNC14 into the membrane, followed by the formation and desorption of mixed micelles. This view is supported by molecular modelling data [11] and is consistent with the second step of the detergent effect described previously [25,26].

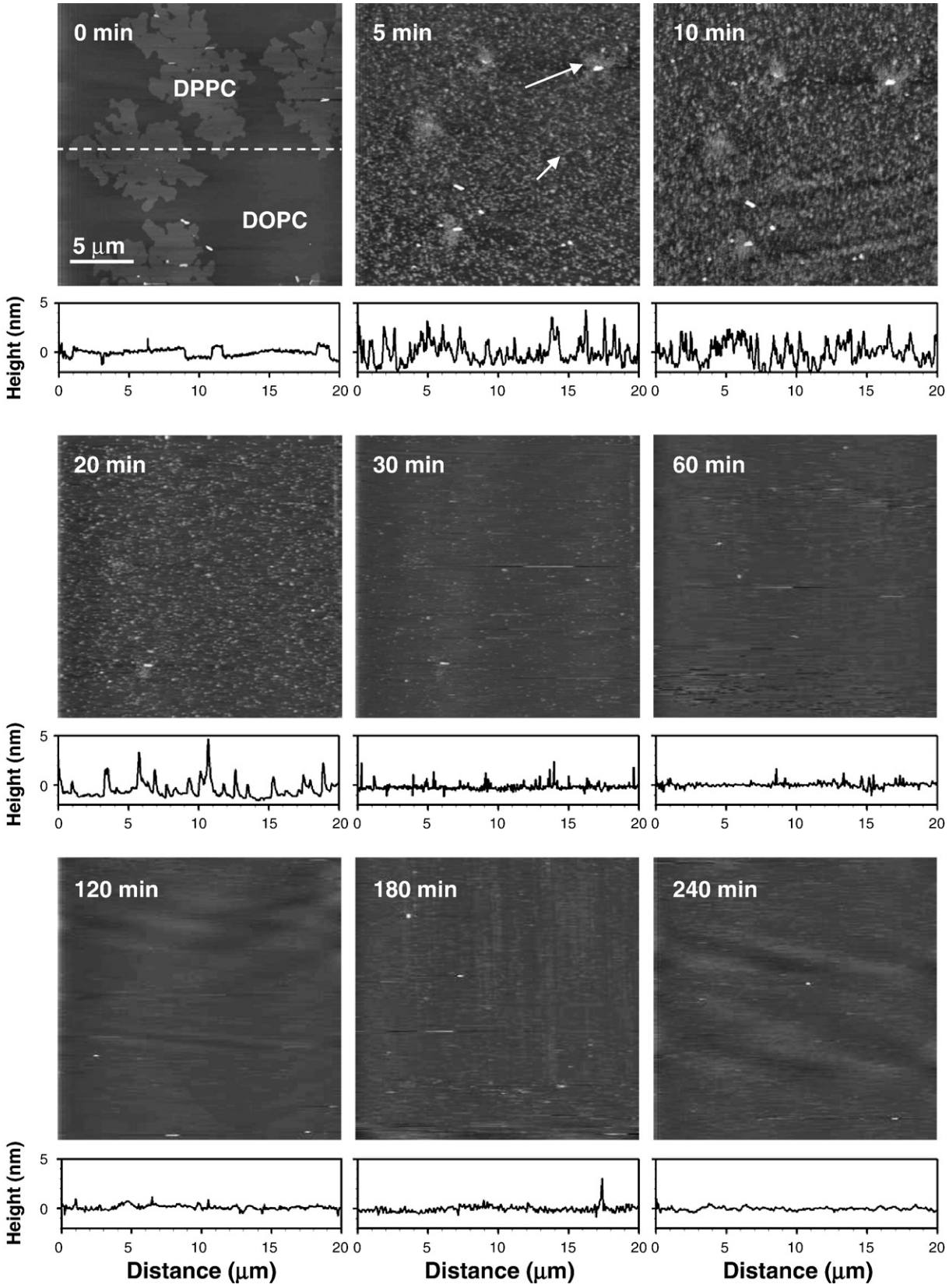

Fig. 2. Nanoscale membrane activity of natural cyclic surfactin. AFM height images (20 μm×20 μm; *z*-scale: 20 nm) of a mixed DPPC/DOPC (1:1, mol/mol) bilayer recorded prior (0 min) and after incubation for 5, 10, 20, 30, 60, 120, 180 and 240 min with SNC14 at 1 mM. For all images, vertical cross-sections were taken along the position indicated by the dashed line at time 0 min. Short and long arrows at 5 min indicate small particles and remaining DPPC islands, respectively.

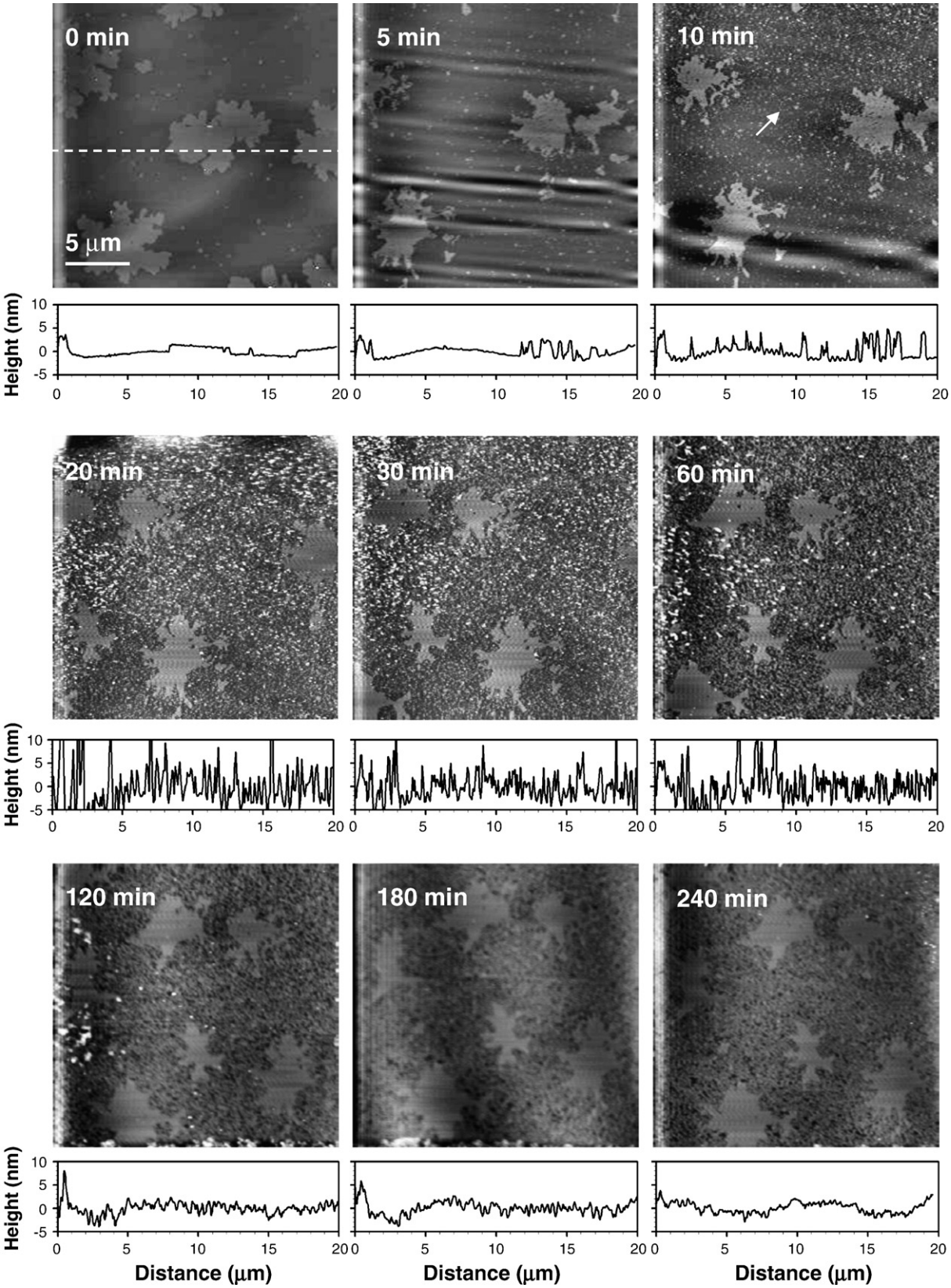

Fig. 3. Influence of the linearization of the peptide cycle. AFM height images (20 μm × 20 μm; *z*-scale: 20 nm) of a mixed DPPC/DOPC (1:1, mol/mol) bilayer recorded prior (0 min) and after incubation for 5, 10, 20, 30, 60, 120, 180 and 240 min with SAL14 at 1 mM. The lower level at 5 min represents the mica surface while the arrow at 10 min indicates small particles.

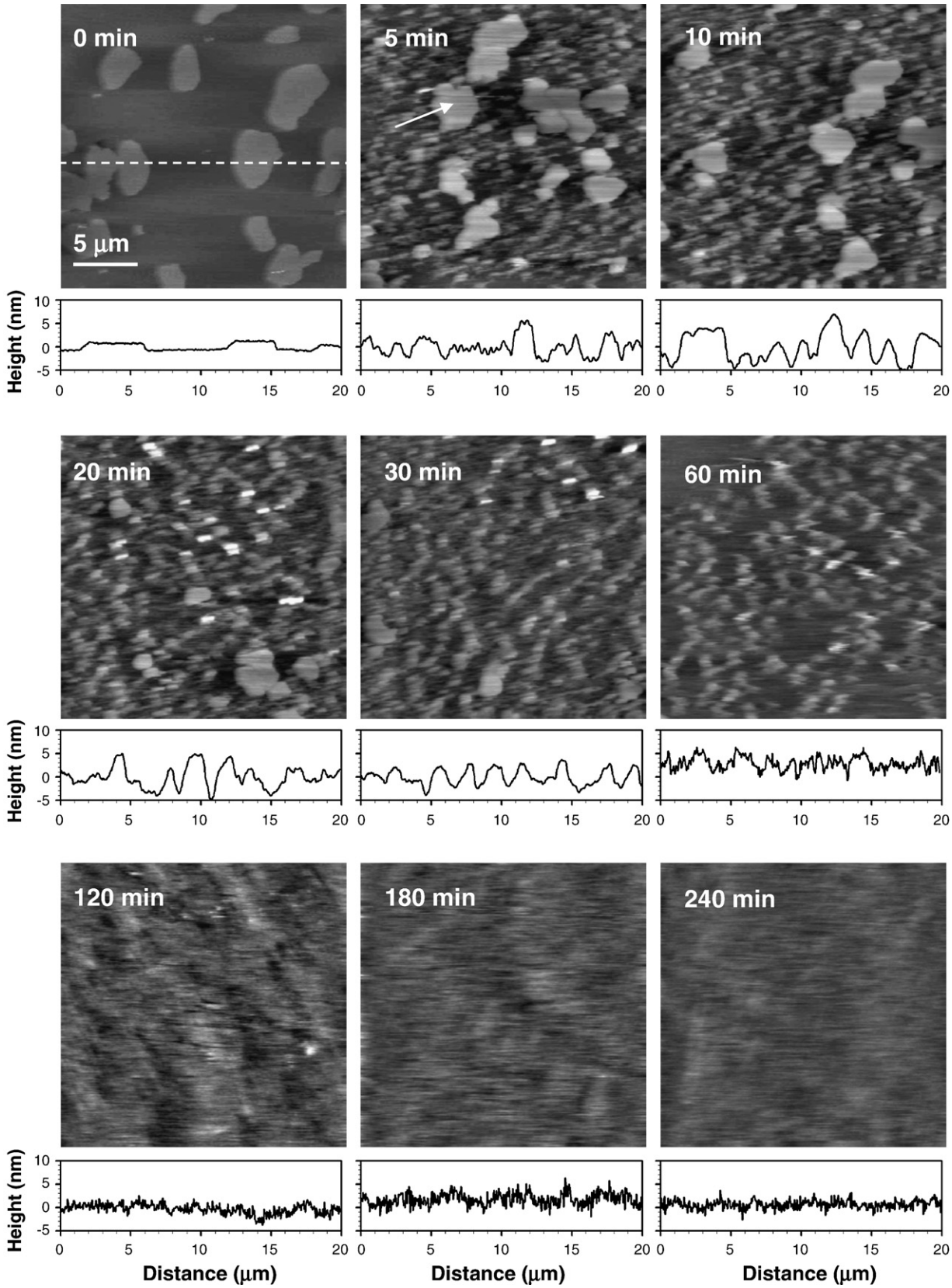

Fig. 4. Influence of the charge. AFM height images (20 μm × 20 μm; *z*-scale: 20 nm) of a mixed DPPC/DOPC (1:1, mol/mol) bilayer recorded prior (0 min) and after incubation for 5, 10, 20, 30, 60, 120, 180 and 240 min with SSL14 at 1 mM. The arrow indicates remaining DPPC domains.

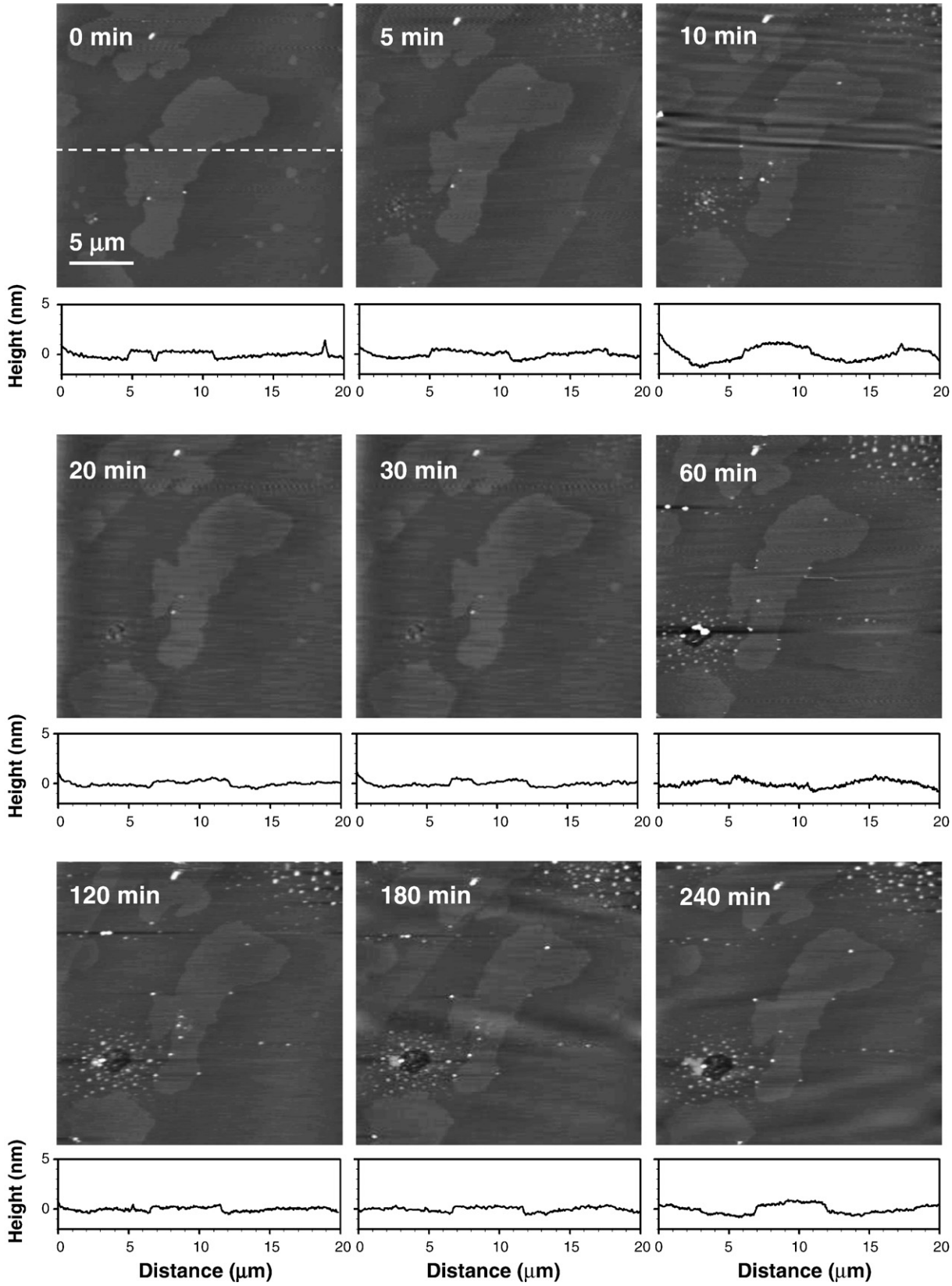

Fig. 5. Influence of the acyl chain length. AFM height images (20 μm × 20 μm; *z*-scale: 20 nm) of a mixed DPPC/DOPC (1:1, mol/mol) bilayer recorded prior (0 min) and after incubation for 5, 10, 20, 30, 60, 120, 180 and 240 min with SSL10 at 1 mM.

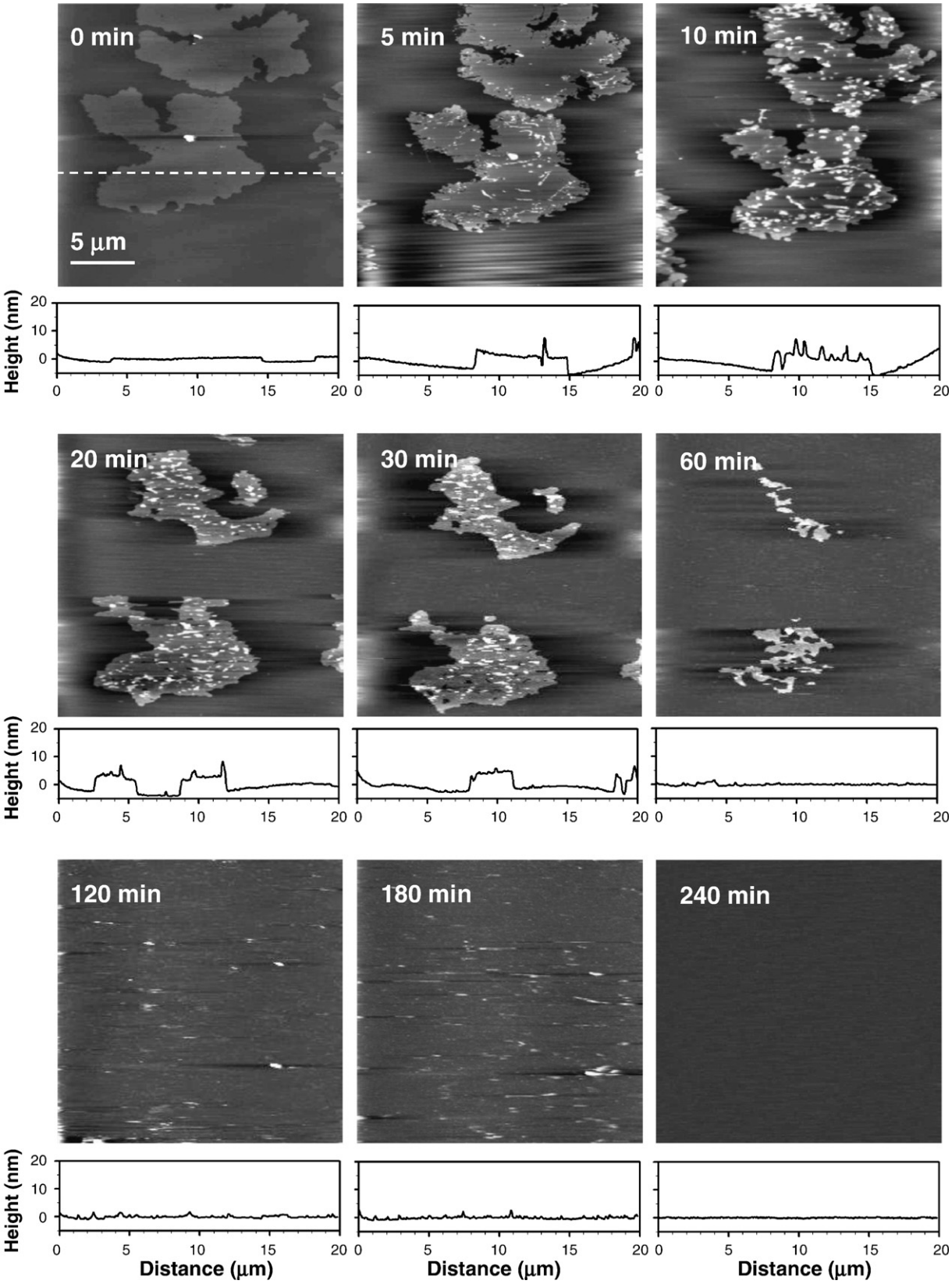

Fig. 6. Influence of the acyl chain length. AFM height images (20 µm × 20 µm; *z*-scale: 20 nm) of a mixed DPPC/DOPC (1:1, mol/mol) bilayer recorded prior (0 min) and after incubation for 5, 10, 20, 30, 60, 120, 180 and 240 min with SSL18 at 1 mM.

3.2. Linear surfactin SAL14 leads to DOPC solubilization and to micelle redeposition

Incubation of DPPC/DOPC bilayers with SAL14 led to a very different behavior (Fig. 3). Progressive solubilization of the DOPC phase leading to the deposition of particles, 5.36±0.31 nm in height (see vertical cross-sections), was observed after 5 min and increased until 60 min. With time, DPPC domains were not affected but redeposition eventually lead to a new phase-separated bilayer. Strikingly, the height difference between the DPPC phase and the newly formed phase was 0.6±0.3 nm, which is substantially smaller than the 1.1 nm DPPC/DOPC height difference. It must be realized that height differences may reflect not only differences in lipid film thicknesses but also of variations in mechanical properties [23]. Nevertheless, we suggest that the resulting newly formed bilayer is likely to contain a mixture of DOPC and SAL14. Thus, in the presence of SAL14, DPPC domains remain resistant to solubilization and lipid/surfactin redeposition occurs. This finding supports the notion that the membrane activity of SAL14 and SNC14 are different, which may be related to the linearization of the peptide cycle of the surfactin and to its higher CMC. The ability of a surfactant to disrupt membranes may be related to two parameters, i.e. the capacity to penetrate into the membrane at low concentrations, and the surfactant to lipid ratio that must be reached to give rise to membrane disruption. The latter parameter can be related to the shape of the molecule: a conical molecule with a large head group introduces a more important constraint in the lipid packing and leads to disruption of the membrane at smaller concentration than rod like molecules.

The formation of bilayers by deposition of mixed phospholipids/detergent micelles is well-documented. For instance, neutron reflection and ellipsometry experiments have shown that mixed micelles composed of dodecyl-maltoside and phospholipids adsorb onto hydrophilic surfaces and that diluting the bulk solution or rinsing with water leads to a gradual removal of detergent molecules leaving a phospholipid-enriched bilayer [27–29]. Also, real-time AFM studies on DPPC/DOPC bilayer systems have shown that the detergent octyl glucoside at high concentration (28 mM > CMC) induces similar solubilization/redeposition [30]. In future AFM work, it would be most interesting to further investigate micelle deposition, particularly the formation of supported bilayers via DOPC/SAL14 vesicle solutions.

3.3. Increasing the surfactin charge leads to DOPC and DPPC solubilization

We explored the possible influence of the charge, by comparing the behavior of SAL14 (2 negative charges) with that of SSL14 (3 negative charges) (Fig. 4). Topographic images of DPPC/DOPC bilayers obtained after incubation for 5, 10, 20, 30, 60, 120, 180 and 240 min with SSL14 at 1 mM revealed a rapid solubilization of DOPC and slower solubilization of DPPC, followed by redeposition leading to a continuous bilayer. The presence of a redeposited bilayer after 240 min is clearly supported by the rough surface morphology, compared to the smooth mica surface (see Fig. 2, 240 min). Hence, the nanoscale membrane activity of SSL14 differs from that of SAL14, in that both DOPC and DPPC were solubilized, leading then to a newly formed bilayer in which DPPC domains are no longer seen.

3.4. Increasing the acyl chain length leads to DOPC and DPPC solubilization, without micelle redeposition

The influence of the length of the surfactin acyl chains was then investigated by comparing the behaviors of SSL10, SSL14 and SSL18, having 10, 14 and 18 carbon atoms, respectively (Figs. 4–6). Comparison of Figs. 4–6 clearly demonstrates that the acyl chain length strongly modulates the nanoscale membrane activity of surfactin. In the presence of 1 mM of the short SSL10 (Fig. 5), the DOPC/DPPC bilayer morphology remained essentially unaltered, even after 240 min, providing strong evidence that short surfactins have poor detergent properties. A reasonable explanation for this is that hydrophobic forces of the SSL10 short acyl chains are too weak to give rise to sufficient insertion into the membrane and to mixed micelle formation, which is indeed reflected in the very high CMC (1114 μM). We also note an increasing number of elevated small particles with time, possibly reflecting peptide aggregates. By contrast, incubation with the long SSL18 led to rapid solubilization of the DOPC phase (Fig. 6), as indicated by the dramatic increase in step height between the lower and higher levels (see cross-sections), and to a time-dependent erosion of the DPPC domains, revealing eventually the clean mica surface. This indicates that, in agreement with its very low CMC (8 μM), SSL18 shows stronger membrane activity than SSL14 since it does not cause micellar redeposition. Interestingly, we note that the behaviors of the SSL18 linear analog and of the SNC14 cyclic surfactin were somewhat similar, suggesting that, at the molecular level, the negative 'geometric effect' (loss of peptide cycle) is compensated by a positive 'hydrophobic effect' (enhanced hydrophobic forces due to longer acyl chains). That the alkyl chain length is important for insertion and micelle formation could be investigated further, using e.g. NMR or molecular modelling.

3.5. DOPC/DPPC bilayers are resistant to solubilization at low surfactin concentration

We also recorded topographic images of bilayers after incubation for 5, 20, and 180 min with SNC14, SAL14, SSL14 and SSL18 at a concentration of 40 μM, which is smaller than the CMC, except for SSL18 (Fig. 7). The three main findings are as follows. First, as for the 1 mM situation, rapid solubilization of the DOPC phase was observed for all surfactins, as indicated by the dramatic increase in step height between the lower and higher levels (see cross-sections). This behaviour is in marked contrast with that of Triton at half the CMC (120 μM) which was shown to have no effect on DOPC phases [24]. Again, this tends to indicate that surfactins have stronger membrane activity than Triton. Second, solubilization of the DPPC domains, previously observed with 1 mM SNC14, SSL14 and SSL 18, was rarely observed at 40 μM, indicating that DPPC domains are resistant to solubilization when the surfactin concentration is low. The resistance to solubilization is directly related to the melting temperature (Tm) of the lipids, which tend to be tightly packed and form gel-phase bilayers [31,32]. Third, partial and complete redeposition was observed with SSL18 and SNC14, as revealed by the decrease in step height between the lower and higher levels, and by the appearance of numerous particles, respectively, while no/poor deposition was noted with SAL 14 and SSL 14. We note that this behavior is opposite to that occurring at 1 mM, indicating that the mechanisms underlying bilayer redeposition by the different surfactins are rather complex and would deserve further investigations using AFM and other complementary techniques. Another direction for future work would be to better understand the nature of the multilayer structures formed at the periphery of the DPPC domains upon treatment with SSL14. Finally, it is worth noting that when SNC14, SAL14, SSL14 and SSL18 were injected at 3 μM, DOPC/DPPC bilayers remained unaltered (data not shown). An interesting direction for future research would be to complement these AFM data using fluorescence techniques with fluorescently-labelled analogs, which would allow to better understand how the surfactins are associating.

4. Conclusions

Using natural cyclic surfactin (SNC14) and four well-defined synthetic analogs (SAL14, SSL14, SSL10 and SSL18), we have shown that the membrane activity of surfactin strongly depends on the geometry of the peptide chain (cyclic vs linear), the number of

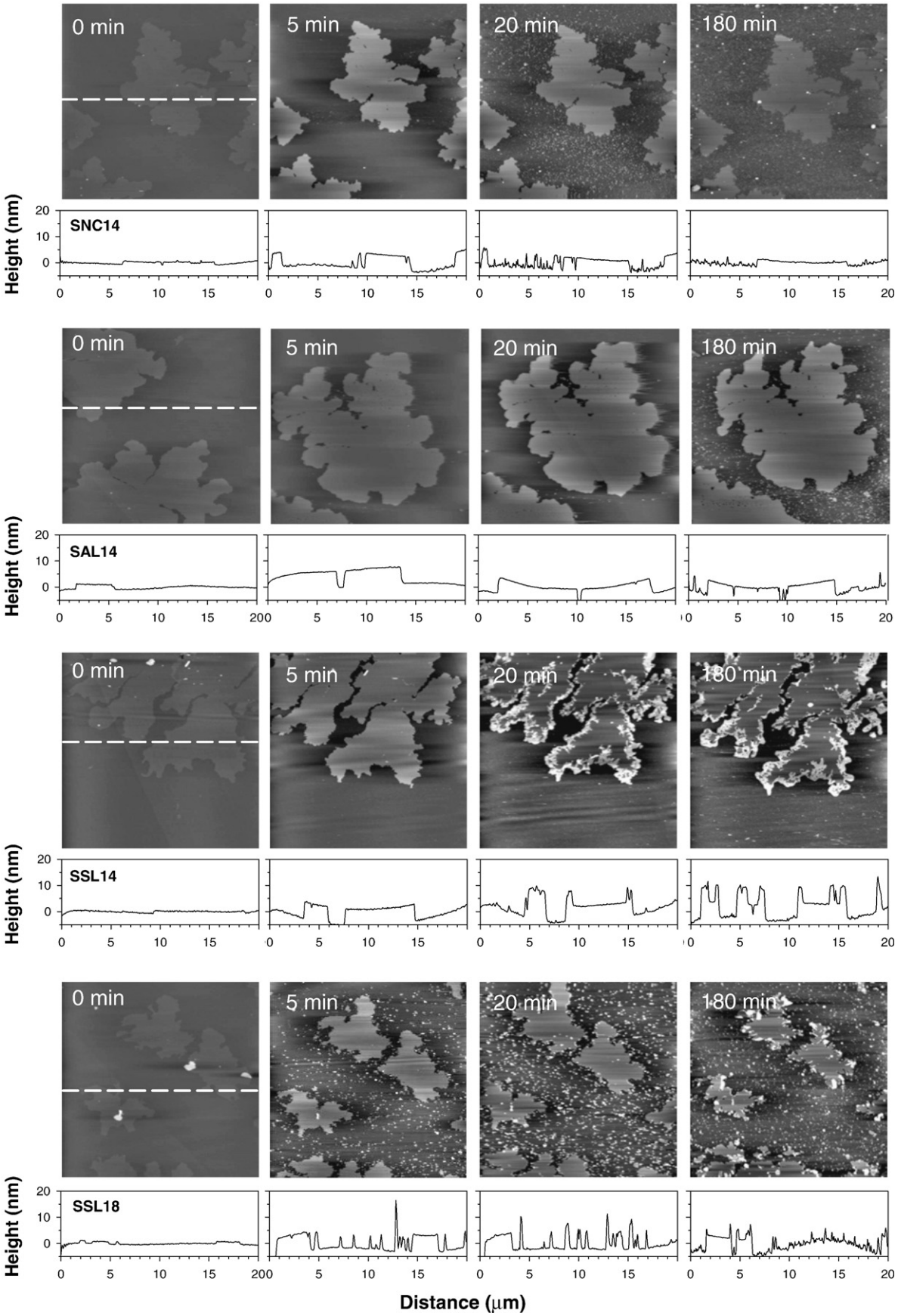

Fig. 7. Influence of the surfactin concentration. AFM height images (20 μm×20 μm; *z*-scale: 20 nm) of mixed DPPC/DOPC (1:1, mol/mol) bilayers recorded prior (0 min) and after incubation for 5, 20, and 180 min with SNC14, SAL14, SSL14 and SSL18 at 40 μM.

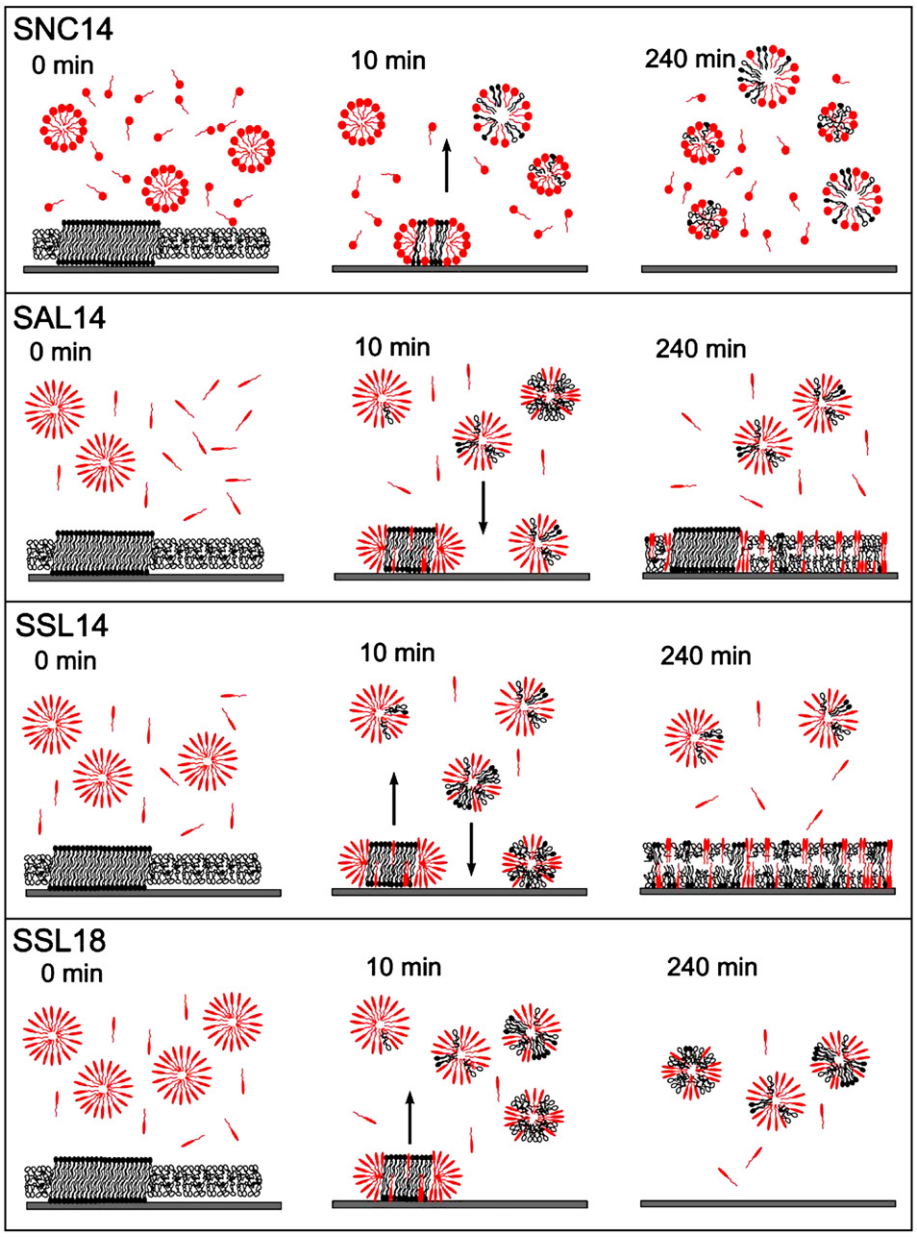

Fig. 8. Molecular models proposed to describe the nanoscale membrane activity of the different surfactins at 1 mM. Molecules in red, with a single tail, represent the different surfactins, while molecules with double tails and either black or white headgroup represent the DPPC and DOPC lipids (see text for details).

negative charges (2 vs 3 carboxylic groups) and the length of the acyl chains (14 vs 10 and 18). As illustrated in Fig. 8, the cyclic SNC14 at 1 mM induces complete solubilization of DOPC/DPPC bilayers, by a mechanism which is likely to involve the rapid insertion of SNC14 into the entire membrane and the desorption of surfactin and lipid molecules, from the mica surface. By contrast, the linear SAL14 is able to solubilize DOPC, not DPPC, and to induce redeposition of surfactin/phospholipid material, leading to a newly formed phase-separated bilayer. This emphasizes the important role played by the molecular geometry. The membrane activity of surfactin is shown to increase with the number of ionic charges: SSL14, which has an additional negative charge, shows somewhat similar effects as SAL14 except that DPPC is slowly solubilized, thereby leading to an homogeneous, newly formed bilayer. Increasing the acyl chain length results in stronger bilayer solubilization without redeposition: the long SSL18 leads to rapid solubilization of the DOPC phase and to a time-dependent erosion of the DPPC domains, without redeposition. Hence, the SSL18 behavior resembles that of SNC14, suggesting that the loss of the peptide cycle is compensated by stronger hydrophobic forces of the longer acyl chains.

This study demonstrates that synthetic analogs represent a valuable tool to study the structure–function relationships of surfactants. The data show that the nanoscale membrane activity of synthetic surfactins may be tuned by modifying their geometry, charge and acyl chain length. In the future, it is expected that such synthetic analogs will find promising applications in the biomedical and biotechnological areas, by enabling the design of new detergents with targeted, well-defined properties.

Acknowledgements

Y.F.D. and M.D. are a Research Associate of the National Foundation for Scientific Research (F.N.R.S.). The support of the of the F.N.R.S., of the Région wallonne, of the Université catholique de Louvain (Fonds

Spéciaux de Recherche), of the Federal Office for Scientific, Technical and Cultural Affairs (Interuniversity Poles of Attraction Programme) and of the Research Department of Communauté Française de Belgique (Concerted Research Action) is gratefully acknowledged. We thank Dr K. El Kirat for valuable discussions.

References

[1] K. Arima, A. Kakinuma, G. Tamura, Surfactin, a crystalline peptide lipid surfactant produced by *Bacillus subtilis*: isolation, characterization and its inhibition of fibrin clot formation, Biophys. Res. Comm. 31 (1968) 488–494.
[2] N. Tsukagoshi, G. Tamura, K. Arima, A novel protoplast bursting factor (surfactin) obtained from *Bacillus subtilis*: the effects of surfactin on *Bacillus megaterium*, Biochim. Biophys. Acta 196 (1970) 204–210.
[3] H. Itokawa, T. Miyashita, H. Morita, K. Takeya, T. Hirano, M. Homma, K. Oka, Structural and conformational studies of [Ile7] and [Leu7] surfactins from *Bacillus subtilis* natto, Chem. Pharm. Bull. 42 (1994) 604–607.
[4] L. Béven, H. Wroblewski, Effect of natural amphipathic peptides on viability, membrane potential, cell shape and motility of mollicutes, Res. Microbiol. 148 (1997) 163–175.
[5] D. Vollenbroich, G. Pauli, M. Özel, J. Vater, Antimycoplasma properties and application in cell culture of surfactin, a lipopeptide antibiotic from *Bacillus subtilis*, Appl. Environ. Microbiol. 63 (1997) 44–49.
[6] D. Vollenbroich, M. Özel, J. Vater, R.M. Kamp, G. Pauli, Mechanism of inactivation of enveloped viruses by the biosurfactant surfactin from *Bacillus subtilis*, Biologicals 25 (1997) 289–297.
[7] M. Kracht, H. Rokos, M. Özel, M. Kowall, G. Pauli, J. Vater, Antiviral and hemolytic activities of surfactin isoforms and their methyl ester derivatives, J. Antibiot. 52 (1999) 613–619.
[8] S. Dufour, M. Deleu, K. Nott, B. Wathelet, P. Thonart, M. Paquot, Hemolytic activity of new linear surfactin analogs in relation to their physico-chemical properties, Biochim. Biophys. Acta 1726 (2005) 87–95.
[9] J.M. Bonmatin, M. Genest, M.C. Petit, E. Gincel, J.P. Simorre, B. Cornet, X. Gallet, A. Caille, H. Labbe, F. Vovelle, M. Ptak, Progress in multidimensional NMR investigations of peptide and protein 3-D structures in solution — from structure to functional-aspects, Biochimie 74 (1992) 825–836.
[10] H. Heerklotz, J. Seelig, Detergent-like action of the antibiotic peptide surfactin on lipid membranes, Biophys. J. 81 (2001) 1547–1554.
[11] M. Deleu, O. Bouffioux, H. Razafindralambo, M. Paquot, C. Hibd, P. Thonart, P. Jacques, R. Brasseur, Interaction of surfactin with membranes: a computational appoach, Langmuir 19 (2003) 3377–3385.
[12] H. Heerklotz, T. Wieprecht, J. Seelig, Membrane perturbation by the lipopeptide surfactin and detergents as studied by deuterium NMR, J. Phys. Chem. 108 (2004) 4909–4915.
[13] H. Heerklotz, J. Seelig, Leakage and lysis of lipid membranes induced by the lipopeptide surfactin, Eur. Biophys. J. 36 (2007) 305–314.
[14] M.C. Giocondi, V. Vié, E. Lesniewska, P.E. Milhiet, M. Zinke-Allmang, C. Le Grimellec, Phase topography and growth of single domains in lipid bilayers, Langmuir 17 (2001) 1653–1659.
[15] M.C. Giocondi, L. Pacheco, P.E. Milhiet, C. Le Grimellec, Temperature dependence of the topology of supported dimirystoyl–distearoyl phosphatidylcholine bilayers, Ultramicroscopy 86 (2001) 151–157.
[16] K. El Kirat, L. Lins, R. Brasseur, Y.F. Dufrêne, Nanoscale modification of supported lipid membranes: synergetic effect of phospholipase D and viral fusion peptides, J. Biomed. Nanotechnol. 1 (2005) 39–46.
[17] K. El Kirat, L. Lins, R. Brasseur, Y.F. Dufrêne, Fusogenic tilted peptides induce nanoscale holes in supported phosphatidylcholine bilayers, Langmuir 21 (2005) 3116–3121.
[18] P.E. Milhiet, M.C. Giocondi, O. Baghdadi, F. Ronzon, B. Roux, C. Le Grimellec, Spontaneous insertion and partitioning of alkaline phosphatase into model lipid rafts, EMBO J. 3 (2002) 485–490.
[19] A. Berquand, M.P. Mingeot-Leclercq, Y.F. Dufrene, Real-time imaging of drug-membrane interactions by atomic force microscopy, Biochim. Biophys. Acta 1664 (2004) 198–205.
[20] J. Mou, J. Yang, C.H. Huang, Z. Shao, Alcohol induces interdigitated domains in unilamellar phospholipid bilayers, Biochemistry (Mosc) 33 (1994) 9981–9985.
[21] M.C. Giocondi, V. Vié, E. Lesniewska, J.P. Goudonnet, C. Le Grimellec, In situ imaging of detergent-resistant membranes by atomic force microscopy, J. Struct. Biol. 131 (2000) 38–43.
[22] Y. Ishigami, M. Osman, H. Nakahara, Y. Sano, R. Ishiguro, M. Matsumoto, Significance of beta-sheet formation for micellization and surface adsorption on surfactin, Colloids Surf. B 4 (1995) 341–348.
[23] Y.F. Dufrêne, W.R. Barger, J.B.D. Green, G.U. Lee, Nanometer-scale surface properties of mixed phospholipid monolayers and bilayers, Langmuir 13 (1997) 4779–4784.
[24] S. Morandat, K. El Kirat, Membrane resistance to Triton X-100 explored by real-time atomic force microscopy, Langmuir 22 (2006) 5786–5791.
[25] J. Lasch, Interaction of detergents with lipid vesicles, Biochim. Biophys. Acta 1241 (1995) 269–292.
[26] U. Kragh-Hansen, M. Le Maire, J.V. Moller, The mechanism of detergent solubilization of liposomes and protein-containing membranes, Biophys. J. 75 (1998) 2932–2946.
[27] F. Tiberg, L. Harwigsson, M. Malmsten, Formation of model lipid bilayers at the silica-water interface by co-adsorption with non-ionic dodecyl maltoside surfactant Eur, Biophys. J. 29 (2000) 196–203.
[28] H.P. Vacklin, F. Tiberg, R.K. Thomas, Formation of supported phospholipid bilayers, via co-adsorption with beta-D-dodecyl maltoside, Biochim. Biophys. Acta 1668 (2005) 17–24.
[29] H.P. Vacklin, F. Tiberg, G. Fragneto, R.K. Thomas, Composition of supported model membranes determined by neutron reflection, Langmuir 21 (2005) 2827–2837.
[30] S. Morandat, K. El Kirat, Solubilization of supported lipid membranes by octyl glucoside observed by time-lapse atomic force microscopy, Colloids and Surfaces 55 (2007) 179–184.
[31] H.A. Rinia, M.M.E. Snel, J.P.J.M. Van der Eerden, B. De Kruijff, Visualizing detergent resistant domains in model membranes with atomic force microscopy, FEBS Lett. 501 (2001) 92–96.
[32] H. Razafindralambo, P. Thonart, M. Paquot, Dynamic and equilibrium surface tensions of surfactin aqueous solutions, J. Surfactants Deterg. 7 (2004) 41–46.